



Original

Renk, O.; Enzinger, R.; Gammer, C.; Scheiber, D.; Oberdorfer, B.; Tkadletz, M.; Stark, A.; Sprengel, W.; Pippan, R.; Eckert, J.; Romaner, L.; Ruban, A.:

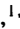

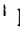





Stainless steel reveals an anomaly in thermal expansion behavior of severely deformed materials.

In: Physical Review Materials. Vol. 5 (2021) 11, 113609.

First published online by APS: 30.11.2021

<https://dx.doi.org/10.1103/PhysRevMaterials.5.113609>

Stainless steel reveals an anomaly in thermal expansion behavior of severely deformed materials

O. Renk ^{1,*}, R. Enzinger ², C. Gammer ¹, D. Scheiber ³, B. Oberdorfer ^{2,†}, M. Tkadletz ⁴, A. Stark ⁵, W. Sprengel ², R. Pippan ¹, J. Eckert ^{1,6}, L. Romaner ⁷, and A. Ruban ^{3,8}¹Erich Schmid Institute of Materials Science, Austrian Academy of Sciences, Jahnstraße 12, 8700 Leoben, Austria²Institute of Materials Physics, Graz University of Technology, Petersgasse 16, 8010 Graz, Austria³Materials Center Leoben Forschung GmbH, Roseggerstrasse 12, 8700 Leoben, Austria⁴Department of Materials Science, Chair of Functional Materials and Materials Systems, Montanuniversität Leoben, Roseggerstraße 12, 8700 Leoben, Austria⁵Institute of Materials Research, Helmholtz-Zentrum Geesthacht, 21502, Geesthacht, Germany⁶Department of Materials Science, Chair of Materials Physics, Montanuniversität Leoben, Jahnstraße 12, 8700 Leoben, Austria⁷Department of Materials Science, Chair of Physical Metallurgy and Metallic Materials, Computational Materials Science, Montanuniversität Leoben, Roseggerstraße 12, 8700 Leoben, Austria⁸Department of Materials Science and Engineering, KTH Royal Institute of Technology, SE-100 44 Stockholm, Sweden (Received 6 September 2021; accepted 8 November 2021; published 30 November 2021)

Thermal expansion of materials is of fundamental practical relevance and arises from an interplay of several material properties. For nanocrystalline materials, accurate measurements of thermal expansion based on high-precision reference dilatometry allow inferring phenomena taking place at internal interfaces such as vacancy annihilation at grain boundaries. Here we report on measurements obtained for a severely deformed 316L austenitic steel, showing an anomaly in difference dilatometry curves which we attribute to the exceptionally high density of stacking faults. On the basis of *ab initio* simulations we report evidence that the peculiar magnetic state of the 316L austenitic steel causes stacking faults to expand more than the matrix. So far, the effect has only been observed for this particular austenitic steel but we expect that other magnetic materials could exhibit an even more pronounced anomaly.

DOI: 10.1103/PhysRevMaterials.5.113609

I. INTRODUCTION

Thermal expansion is an elementary materials behavior, being not only of interest from a fundamental theoretical point of view, but also of practical relevance in engineering. For instance, differences in the thermal expansion coefficient of components or material combinations may lead to residual stresses and damage or failure in service. Understanding and tailoring thermal expansion is thus of great importance. In this context, a prominent example are Invar alloys, i.e., Fe-Ni alloys of a specific concentration with a close to zero expansion within a certain temperature range [1–4]. Apart from alloying, thermal expansion can also be affected by lattice defects. Lattice defects are associated with an excess volume which possibly affects the global thermal expansion when annealing out upon thermal excitation. However, given the rather small excess volume, sufficient measurement resolution or large defect populations are required to reveal an effect.

High-precision difference dilatometry is a powerful method, which enables the determination of the tiniest absolute length changes. This technique allows one to study defect annihilation kinetics [5,6] and early stages of precipitation (e.g., decomposition or clustering) [7,8], and can

even reveal the grain boundary (GB) excess volume [9] or the vacancy relaxation volume [10]. Difference dilatometry relies on the excess volume associated with crystal defects, compared to the perfect lattice (reference sample), which may be released upon annealing the sample. To determine the mentioned quantities or to reveal how this excess volume affects thermal expansion, the length of a pristine, defect-scarce reference and its evolution with temperature is compared to a sample containing an abundance of lattice defects. When defects and annihilation sites are present in sufficiently large quantities, the release of their specific excess volume can induce a measurable volume or length change, thereby enabling their investigation. Nanostructured materials prepared by high-pressure torsion (HPT) are ideal materials for such studies as HPT introduces high densities of lattice defects into bulk materials by applying strains of several thousand percent, accompanied by grain refinement down to the 100 nm regime or even less [11]. Such bulk nanomaterials have been intensively studied in recent years and instrumental improvements of high-precision difference dilatometers have provided the necessary spatial resolution and thermal drift stability for the length measurements [12].

These measurements have revealed for severely deformed pure metallic materials a distinct difference of the relative length change between a defect-containing and well-annealed reference once lattice defects annihilate [5,10]. Depending on the sample orientation, this relative length change can either be positive or negative, i.e., enhance or reduce thermal expansion.

*Corresponding author: oliver.renk@oeaw.ac.at

†Present address: Austrian Foundry Research Institute, Parkstraße 21, A-8700 Leoben, Austria.

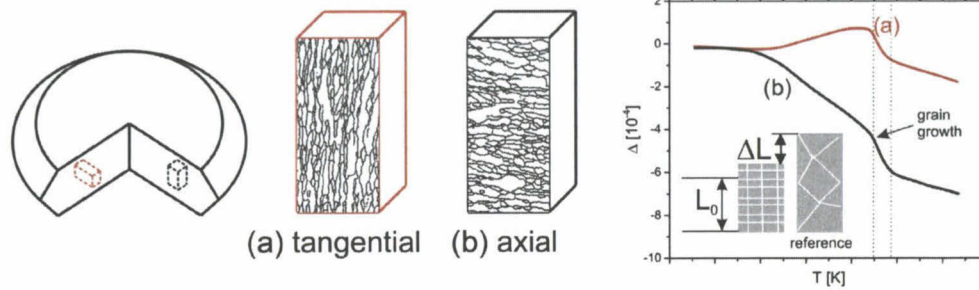


FIG. 1. Schematics illustrating the anisotropic relative length change, Δ , measured in severely deformed single-phase alloys. Due to the elongated grain shape of HPT processed samples, the short grain axis is once aligned perpendicular to the measurement direction (a), while being parallel to it in the other case (b). The grain structure is not to scale.

sion [10] (cf. Fig. 1). A negative relative length change does not imply shrinkage of the sample but only a reduced thermal expansion compared to the almost defect-free reference. The anisotropy of the length change is present only at moderate annealing temperatures where the grain size remains stable. Thus it has been ascribed to the anisotropic annihilation of excess vacancies [10], originating from the elongated grain shape, inherently present in severely deformed metals [13]. As vacancy annihilation at the GBs occurs by self-diffusion processes, they will migrate along the shortest path to reach the boundaries. Depending on the orientation of the elongated structure with respect to the dilatometric sample, these annihilation processes will either induce a positive or negative length change, Fig. 1. Similar length changes were observed for a variety of severely deformed single-phase nanostructures and are accepted to be generally valid, as long as only defect relaxation occurs while other processes such as precipitation remain absent [7,8], Fig. 2.

In stark contrast, we measured a fundamentally different trend for a severely deformed, nanocrystalline (NC) austenitic steel. Independent of the measurement direction, a positive relative length change was observed, although for the investigated temperature range spinodal decomposition or precipitation can be excluded [14,15]. A yet unknown expansion mechanism needs to be active. We propose that this intriguing effect arises from the high density of stacking

faults (SFs) introduced by the HPT process. The particular chemical composition of this stainless steel further leads to a low-to-high spin transition in the SF which causes an increased thermal expansion of the SF compared to the perfect fcc bulk. To prove this hypothesis, we repeated the experiments on other materials with low stacking fault energies (SFEs, i.e., similar SF densities) which do not show this anomaly.

II. EXPERIMENTAL METHODS

NC fcc structures of selected materials were prepared using quasiconstrained HPT [11,16]. Disks 30 mm in diameter and 8 mm in height were processed under an applied nominal pressure of 3.5 GPa for 15 rotations at a rotational speed of 0.07 rpm. The according equivalent von Mises strains ($\epsilon_{VM} > 40$ for radii where dilatometric samples were extracted) are sufficient to achieve homogeneous grain and defect structures [17,18]. Four materials were investigated, Cu37Zn (α -brass); Co40Ni; and two austenitic steel grades, a 316L steel (grade A220) and a nitrogen-alloyed austenite (grade P555), both from voestalpine Böhler Edelstahl, Austria. Chemical compositions of the austenites are listed in Table I while the alloying contents of the copper and cobalt alloys are given in at. % above. Besides the large alloying content (>30 at. %), all materials have an extremely low SFE ($\gamma_{SFE} \sim 20 \text{ mJ m}^{-2}$)

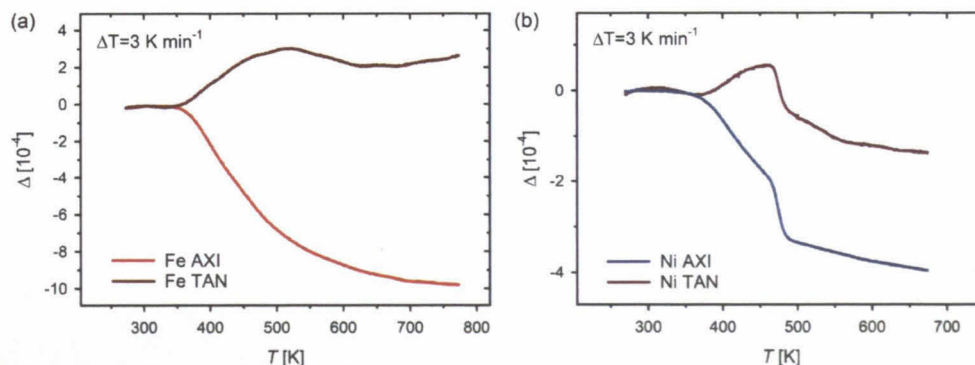


FIG. 2. Examples for length changes upon linear heating for severely deformed Fe (a) and Ni (b). Depending on the sample orientation qualitatively similar anisotropic length changes are observed.

TABLE I. Chemical composition of the two austenitic steels (at. %).

	Cr	Ni	Mn	Mo	Si	N	C	Fe
316L	18.8	13.8	1.7	1.6	0.6	0.3	0.1	Balance
P555	19.0	0.8	19.5	0.1	0.6	2.3	0.2	Balance

[19–21]. Severe plastic deformation of metals with low SFE at low homologous temperatures is known to produce nanostructures with high densities of SFs [19,22]. Hence, these specimens are perfectly suited to prove the introduced hypothesis that the local fcc to hcp transition of the SF induces the discussed phenomenon in the NC 316L steel.

The nanostructures were analyzed in the radial direction of the HPT disk using conventional and high-resolution (HR) transmission electron microscopy (TEM). TEM samples were prepared using standard grinding and polishing followed by electropolishing to thin the samples to transparency. A C_s -corrected TEM (JEOL 2100F) operated at 200 kV was used. Average SF densities were calculated from the HR TEM images. Samples for dilatometry (5.65 mm diameter, 4 mm height) were extracted from the HPT disk along two directions using electric discharge machining. For one set the cylinder axis was oriented parallel to the former torsion axis (AXI samples) while for the other one the axis was oriented parallel to the tangential (TAN samples) direction (Fig. 1). These orientations were chosen as they exhibited maximum anisotropy of the relative length change [10], Fig. 2.

Difference dilatometry measurements have been performed in two measurement modes and by applying two different dilatometers. A high-resolution noncontact laser dilatometer, which determines length changes on the basis of Michelson interferometry, has been applied to study several 316L steel AXI and TAN samples, an AXI Co40Ni sample as well as an AXI nitrogen-alloyed austenite (P555) sample. In each case, a heating rate of 3 K min^{-1} has been used in order to attain temperatures of at least 1130 K at a pressure of $< 10^{-5}$ mbar. By performing *in situ* annealing for at least 2 h after heating the respective samples to this maximum temperature and recording in each case just another measure-

ment with the same heating rate for the now well-annealed samples, they serve as their own references, thereby minimizing device related errors. Further details for this dilatometer can be found elsewhere [12]. A high-precision dual push-rod dilatometer (Linseis L75VD500LT) was applied to conduct measurements in the temperature range up to 773 K at TAN and AXI Cu37Zn samples with a heating rate of 3 K min^{-1} as well as at AXI 316L steel samples with an order of magnitude reduced heating rate (0.3 K min^{-1}). In this case, reference samples were measured simultaneously, which had been obtained previously by annealing samples of each material in a vacuum furnace ($< 10^{-5}$ mbar) at temperatures larger than $0.7 T_m$ to remove any deformation induced defects.

As an input for the *ab initio* calculations, the lattice parameter of the two austenitic steels was determined using *in situ* synchrotron x-ray diffraction (XRD) measurements at the high-energy beamline P07 at DESY (PETRA III, Hamburg, Germany). A thermocouple was directly attached onto the samples (3.8 mm diameter, 7.9 mm height) which were inductively heated in high vacuum ($< 10^{-4}$ mbar) up to 1073 K at a rate of 5 K min^{-1} . Diffraction patterns were collected in transmission geometry every 0.5 K at a photon energy of 87.1 keV using a PerkinElmer XRD 1621 flat panel detector. A LaB6 line position standard of SRM 660c type provided by the National Institute of Standards and Technology was used for calibration. The two-dimensional (2D) diffraction data were azimuthally integrated and the obtained one-dimensional (1D) diffractograms were evaluated by means of a sequential peak fitting procedure (Bruker TOPAS 6 software). Temperature-dependent lattice parameters were determined from the peak positions of eight individual *hkl* reflections (111, 200, 220, 311, 222, 400, 331, and 420).

III. EXPERIMENTAL RESULTS

In the as-HPT deformed state all specimens consist of NC grains ($< 100 \text{ nm}$ grain size), slightly elongated along the tangential direction, shown for the 316L steel in Fig. 3(a). Plenty of SFs can be observed inside the grains, Figs. 3(b) and 3(c). On average a SF is found every 1.8 nm in the case of the 316L steel. The temperature-dependent lattice parameters of

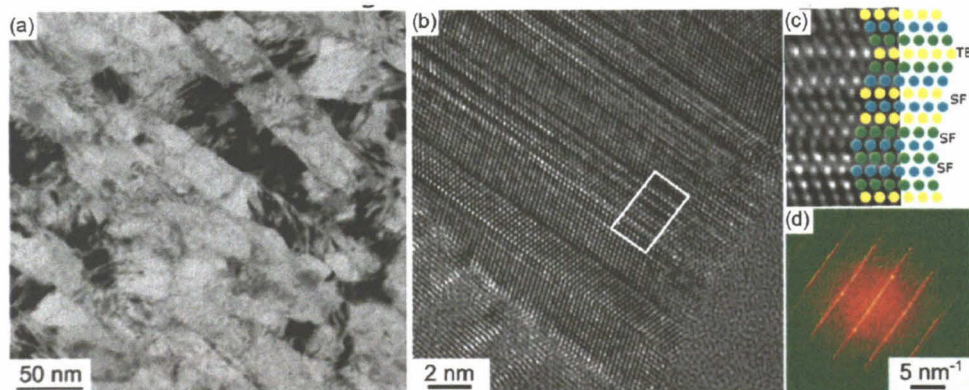


FIG. 3. (a) Bright-field TEM and (b) HR TEM images of the severely deformed 316L steel. (c) A small area is overlaid with the atomic model of the stacking sequence, revealing the presence of a twin boundary (TB) and multiple SFs. (d) The streaks in the corresponding FFT confirm the high density of SFs.

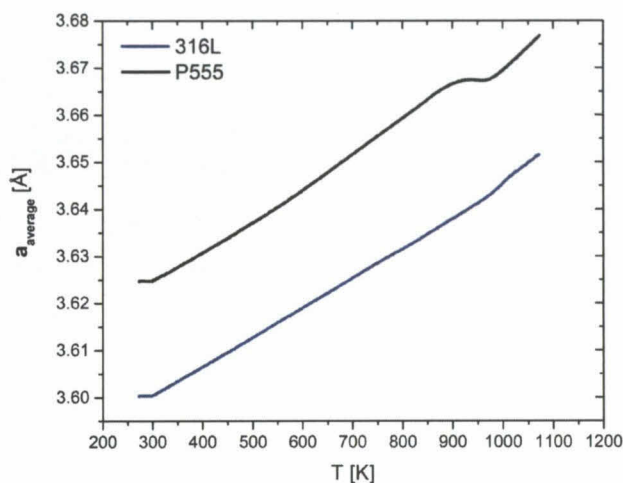


FIG. 4. Temperature dependence of the lattice parameter of the two austenitic steels measured from *in situ* synchrotron XRD experiments.

the two austenitic steels differ remarkably, Fig. 4. The lattice parameter of the nitrogen-alloyed steel is about 1% larger than for the 316L steel, which also has a slightly lower thermal expansion, Fig. 4.

The results of the dilatometric measurements are summarized in Fig. 5. For all samples investigated, the relative length change,

$$\Delta = \left(\frac{\Delta L}{L_0} \right)_{\text{HPT}} - \left(\frac{\Delta L}{L_0} \right)_{\text{REF}}, \quad (1)$$

is plotted as a function of temperature. $(\Delta L/L_0)_{\text{HPT}}$ is the length change of the HPT specimen while $(\Delta L/L_0)_{\text{REF}}$ is the length change of the reference sample when heated to the targeted temperature.

For the brass samples the typical anisotropic behavior—a positive relative length change for the TAN and a negative relative length change for the AXI samples—well known for single-phase materials is observed. The onset of grain growth above 473 K can be clearly distinguished (Fig. 5).

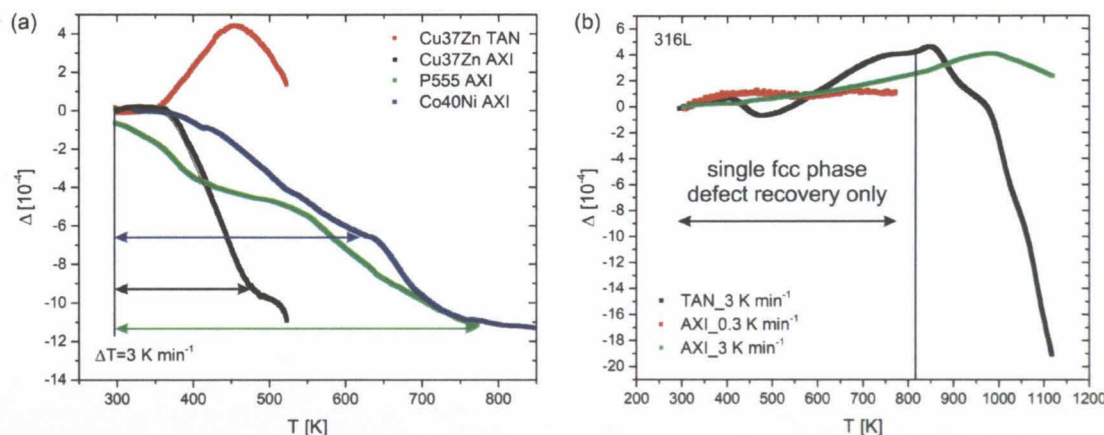


FIG. 5. Relative length changes of the various HPT deformed samples measured by high-precision difference dilatometry as a function of temperature. The temperature ranges of interest where only defect recovery without grain growth occurs is indicated with arrows.

It should be noted that only this recovery region where the grain size remains stable is of interest for the observed phenomenon. These temperature ranges are highlighted with arrows in Fig. 5. Although the absolute values differ, identical trends were measured for the Co40Ni samples. In contrast, for the NC 316L steel, for both specimen orientations a positive relative length change is observed in the recovery regime ($T < 823$ K). Only for higher temperatures where grain growth occurs a negative relative length change can be measured, with the onset temperatures differing for the two specimen orientations. This temperature range is, however, not in the focus of the present study. While vacancy annihilation and recovery processes certainly proceed also in these samples, another process needs to counterbalance these effects and the associated negative length change for the AXI orientation. Although earlier microstructural investigations, including TEM and atom probe tomography (APT) exclude precipitation for short-term anneals up to 823 K [14,15], nanocluster formation may have been missed. For clarification, another AXI sample of the 316L austenitic steel was heated with an order of magnitude reduced heating rate (0.3 K min^{-1}). If cluster formation or precipitation would cause the unexpected positive length change, the onset temperatures of the curves should be clearly shifted, which is not the case. The curves remain identical, indicating a different origin of this phenomenon [Fig. 5(b)].

Although all investigated samples have a low SFE and hence high densities of SFs inside the NC grains, a positive relative length change for both sample orientations was only observed for the 316L steel, suggesting it to be a peculiarity of iron-based alloys. However, also for the nitrogen-alloyed austenite (P555), the typical measurement curve (i.e., a negative relative length change for the AXI samples), also observed for the Co40Ni and brass samples, was recorded.

IV. ATOMISTIC CALCULATIONS/METHODS AND RESULTS

As within the testing temperature range all investigated alloys are homogeneous single-phase metals, the abnormal expansion behavior of the severely deformed 316L should be

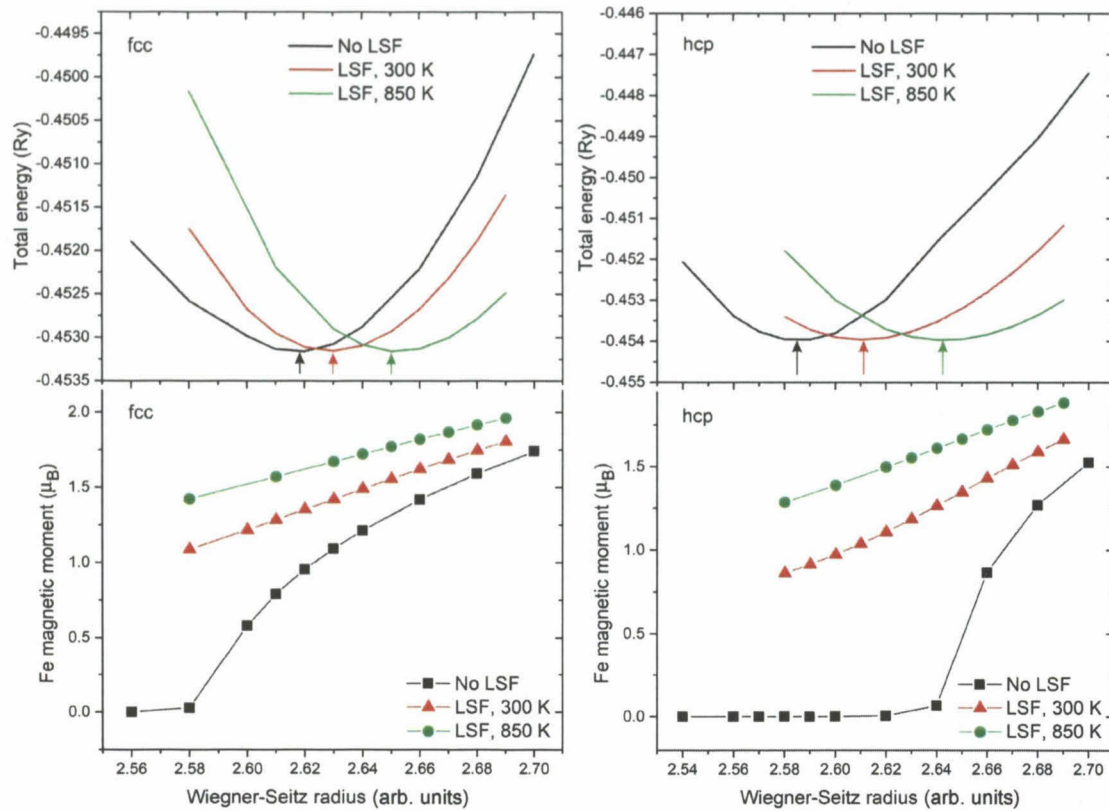


FIG. 6. Total energy (top row) and magnetic moment of Fe (bottom row) as a function of the Wigner-Seitz radius for the hcp and fcc structure without LSF and when including LSF at different temperatures. Vertical arrows in the top row indicate the thermal expansion induced by LSF.

connected to some specific properties of the SFs, present in large amounts at the atomic scale. This specific property is, further, material and composition dependent, as the peculiar effect was only observed for the 316L but not for the P555 steel. Since a SF can be considered as an atomically thin hcp phase in the fcc crystal being mostly oriented parallel to the shear direction (Fig. 3), this effect might be traced to some specific behavior of the hcp structure. Namely, the abnormal expansion could result from a larger thermal expansion of the hcp compared to the fcc phase, counteracting the expected shrinkage for the AXI samples.

To test this assumption, we conducted *ab initio* simulations for the 316L steel focusing on the contribution of magnetic and electronic excitations to the thermal expansion. In fact, the paramagnetic state of austenitic steels [23] is largely dominated by longitudinal spin fluctuations (LSFs), leading to a substantial increase of the local magnetic moments of all 3d metals at finite temperature, which are otherwise zero—as for Ni and Cr—or relatively small, as for Fe and Mn (see Refs. [24,25]). The influence of LSFs on the lattice expansion is studied with *ab initio* calculations for the 316L steel by the exact muffin-tin orbital (EMTO) method [26,27] using a coherent potential approximation (CPA) [28–30], as implemented in the Lyngby version of the code and the locally self-consistent Green's function (ELSGF) technique [31–33], which considers random alloys within a realistic supercell approach. The small amounts of interstitial N and C and of

substitutional Si were neglected. In the ELSGF calculations 864- and 768-atom supercells for the fcc and hcp phase were used. ELSGF calculations were used to tune and test the corresponding EMTO CPA calculations. The self-consistent calculations were done using local density approximation [34], while the final total energies have been obtained using the PBE generalized gradient approximation [35]. Integration over the Brillouin zone was done by using a $31 \times 31 \times 31$ equidistant grid of points for the fcc, and a $31 \times 31 \times 19$ grid for the hcp structure. All calculations used the Green's function formalism which allows an accurate account of one-electron excitations at finite temperature with the use of the Fermi-Dirac function. The magnetically disordered configuration of the local spins was considered using the coherent potential approximation for DLM, while the free energy contribution from LSF can be obtained as [36]

$$F_{\text{LSF}} = k_B T \sum_i d_i c_i \ln [(m_i(a, T))], \quad (2)$$

where c_i is the concentration of the i th element in the alloy, m_i its local magnetic moment for lattice constant a and temperature T , and d_i is the prefactor, depending on the degree of spin localization. It is 3 for very weak or absent localization (Ni, Cr, and Mn in hcp structures), 1 for pronounced localization (Fe in fcc structure), and 2 for intermediate cases (Mn in fcc, Fe in hcp structure). This expression for the free energy is an approximation; however, more accurate treatments would re-

quire going beyond density functional theory (DFT) which is practically impossible for complicated random alloy systems.

Employing this methodology, the contribution to the lattice expansion from LSF was evaluated between 300 and 850 K, Fig. 6. There, the change in total energy with the Wigner-Seitz (WS) radius is shown together with the corresponding magnetic moment on the Fe atom, which illustrates important differences in the magnetic state. Without LSF (black) the disordered magnetic state would not exhibit any temperature dependence. The moment is essentially zero for the hcp structure while it is sizable, about 0.75 Bohr magnetons, for the fcc structure. This pronounced difference in the moments is reflected in the lattice parameter, which is distinctively smaller for the hcp compared to the fcc structure. When including LSF, the moment increases with temperature and the minimum of the total energy curve shifts towards higher WS radii, indicative of lattice expansion. Note that in the present calculations this expansion is solely driven by LSF. For hcp, the increase in moment is more pronounced compared to fcc and, therefore, also the expansion effect is much stronger; see vertical arrows in Fig. 6. The linear coefficient of thermal expansion, α , arising from LSF alone can thus be estimated to be 14×10^{-6} and 23×10^{-6} for the fcc and hcp phases, respectively. Hence the hcp structure experiences a much stronger contribution to the lattice expansion than the fcc phase. Applying this result to the quantity Δ determined in dilatometry, we assume the extreme case of a fully hcp HPT sample (i.e., a SF on every second lattice plane). In this way, an upper limit for the effect is obtained. The actual SF density is certainly smaller than this, but not significantly. Inserting the results obtained for the linear expansion coefficient into Eq. (1) we obtain $\Delta = 0.005$ for the 316L steel when heating from 300 to 850 K. This is higher than the shrinkage effect commonly observed for the AXI samples (e.g., $\Delta = -0.0012$ for P555 or CoNi in this temperature range) where no pronounced difference between the fcc and hcp phase is assumed. Hence, it is plausible that the LSF effect compensates the expected shrinkage from vacancies.

V. DISCUSSION AND CONCLUSIONS

High-precision difference dilatometry revealed an unexpected anomaly of the thermal expansion behavior of a severely deformed 316L steel. Contrary to other severely deformed single-phase materials, even the AXI samples exhibited a positive relative length change. However, compared to HPT deformed single-phase metals studied so far, also the deformed structure of the 316L steel differs. Apart from the large alloying content, the NC 316L contains large densities of SFs. While this also holds true for the other materials investigated here, the performed atomistic calculations indicate that the SFs in the case of the 316L steel may indeed induce a different behavior which we assign to LSF. Why other effects, potentially explaining the anomaly, can be excluded shall be discussed in the following. This includes (i) vibrational excitations, (ii) chemical decomposition, and (iii) GB segregation.

Regarding (i), vibrational contributions to the thermal expansion for fcc and hcp phases are considered approximately the same, and do not play a dominant role. Unfortunately, a di-

rect theoretical confirmation connected to the modeling of the vibrational free energy in these alloys in a finite temperature magnetic state is out of reach. However, *ab initio* calculations of the SFE and its temperature dependence without considering the vibrational contribution in fcc Fe alloys agree closely with experimental data, indicating that the vibrational free energies of the fcc and hcp phases are similar [24,37]. The absence of the anomaly for all other alloys containing high densities of SFs, where the vibrational effect could arise as well, further supports this assumption. Regarding (ii) it is worth noting that a positive relative length change was found for precipitation sequences (e.g., in Al alloys) [8]. However, up to temperatures of 823 K earlier APT and TEM investigations exclude precipitation or second phase formation during short-term annealing treatments [14,15]. Only at higher temperatures (~ 1073 K) does a second phase form. This is supported by the XRD patterns obtained during *in situ* heating experiments to deduce the lattice parameter, indicating for the 316L steel up to 823 K only the presence of the fcc phase. The APT data further exclude spinodal decomposition as origin of the unexpected positive length change of the NC 316L samples. Finally, regarding (iii), although APT revealed Si segregation to the GBs upon annealing [14,15], it can be excluded as a possible mechanism. To check this, DFT calculations employing a methodology described earlier were performed [38]. Our model considers the $\Sigma 5[100](013)$ CLS GB in the ferromagnetic state, expected to exhibit trends similar to GBs in 316L, since the atomic volume of the matrix atoms is comparable between the bcc and fcc crystal. Si has a smaller volume as the matrix and a trend to occupy GB positions which are compressed with respect to the bulk. This leads to shrinkage due to segregation, similarly to what is expected for vacancy segregation, excluding segregation as the reason for the anomaly.

In conclusion, we identified a yet unknown expansion mechanism in a severely deformed stainless steel. The peculiar magnetic structure of the 316L steel causes a large thermal expansion of SFs normal to the fault plane. Other low-SFE materials do not show this anomalous expansion mechanism, since hcp and fcc structures behave similarly. Our results promote the understanding of paramagnetic austenitic steels, in particular the coupling between magnetic state and volume. This coupling, responsible for Invar and anti-Invar behavior, also acts at SFs and is strong enough to counteract the conventionally observed shrinkage of severely deformed materials due to vacancy annihilation. We expect that the 316L steel is not the only system showing this effect. Careful *ab initio* screening of compositionally complex alloys should be carried out to find compositions which may show an even stronger anomalous expansion. We leave such investigations to future efforts.

ACKNOWLEDGMENTS

O.R. acknowledges funding from the Austrian Academy of Sciences via Innovation Fund Grant No. IF 2019-37. The authors A.R. and D.S. gratefully acknowledge financial support under the scope of the COMET program within the K2 Center “Integrated Computational Material, Process and Product Engineering (IC-MPPE)” (Project No. 859480). This

program is supported by the Austrian Federal Ministries for Climate Action, Environment, Energy, Mobility, Innovation and Technology (BMK) and for Digital and Economic Affairs

(BMDW), represented by the Austrian research funding association (FFG), and the federal states of Styria, Upper Austria, and Tyrol.

- [1] C. É. Guillaume, *Recherches sur les aciers au nickel*, *J. Phys. Theor. Appl.* **7**, 262 (1898).
- [2] M. Shiga, *Invar alloys*, *Curr. Opin. Solid State Mater. Sci.* **1**, 340 (1996).
- [3] T. Moriya and K. Usami, *Magneto-volume effect and Invar phenomena in ferromagnetic metals*, *Solid State Commun.* **88**, 911 (1993).
- [4] M. Van Schilfgaarde, I. A. Abrikosov, and B. Johansson, *Origin of the Invar effect in iron-nickel alloys*, *Nature (London)* **400**, 46 (1999).
- [5] G. Reglitz, B. Oberdorfer, N. Fleischmann, J. A. Kotzurek, S. V. Divinski, W. Sprengel, G. Wilde, and R. Würschum, *Combined volumetric, energetic and microstructural defect analysis of ECAP-processed nickel*, *Acta Mater.* **103**, 396 (2016).
- [6] B. Oberdorfer, B. Lorenzoni, K. Unger, W. Sprengel, M. Zehetbauer, R. Pippan, and R. Würschum, *Absolute concentration of free volume-type defects in ultrafine-grained Fe prepared by high-pressure torsion*, *Scr. Mater.* **63**, 452 (2010).
- [7] R. Enzinger, E. Hengge, W. Sprengel, and R. Würschum, *High-precision isothermal dilatometry as tool for quantitative analysis of precipitation kinetics: Case study of dilute Al alloy*, *J. Mater. Sci.* **54**, 5083 (2019).
- [8] L. Resch, G. Klinsner, E. Hengge, R. Enzinger, M. Luckabauer, W. Sprengel, and R. Würschum, *Precipitation processes in Al-Mg-Si extending down to initial clustering revealed by the complementary techniques of positron lifetime spectroscopy and dilatometry*, *J. Mater. Sci.* **53**, 14657 (2018).
- [9] E. M. Steyskal, B. Oberdorfer, W. Sprengel, M. Zehetbauer, R. Pippan, and R. Würschum, *Direct Experimental Determination of Grain Boundary Excess Volume in Metals*, *Phys. Rev. Lett.* **108**, 055504 (2012).
- [10] J. A. Kotzurek, E. M. Steyskal, B. Oberdorfer, A. Hohenwarter, R. Pippan, W. Sprengel, and R. Würschum, *Direct measurement of vacancy relaxation by dilatometry*, *Appl. Phys. Lett.* **109**, 021906 (2016).
- [11] A. P. Zhilyaev and T. G. Langdon, *Using high-pressure torsion for metal processing: Fundamentals and applications*, *Prog. Mater. Sci.* **53**, 893 (2008).
- [12] M. Luckabauer, W. Sprengel, and R. Würschum, *A high-stability non-contact dilatometer for low-amplitude temperature-modulated measurements*, *Rev. Sci. Instrum.* **87**, 075116 (2016).
- [13] O. Renk, P. Ghosh, and R. Pippan, *Generation of extreme grain aspect ratios in severely deformed tantalum at elevated temperatures*, *Scr. Mater.* **137**, 60 (2017).
- [14] O. Renk, A. Hohenwarter, K. Eder, K. S. Kormout, J. M. Cairney, and R. Pippan, *Increasing the strength of nanocrystalline steels by annealing: Is segregation necessary?*, *Scr. Mater.* **95**, 27 (2015).
- [15] O. Renk, A. Hohenwarter, B. Schuh, J. H. Li, and R. Pippan, *Hardening by annealing: Insights from different alloys*, *IOP Conf. Ser.: Mater. Sci. Eng.* **89**, 12043 (2015).
- [16] A. Vorhauer and R. Pippan, *On the onset of a steady state in body-centered cubic iron during severe plastic deformation at low homologous temperatures*, *Metall. Mater. Trans. A* **39**, 417 (2008).
- [17] R. Pippan, S. Scheriau, A. Taylor, M. Hafok, A. Hohenwarter, and A. Bachmaier, *Saturation of fragmentation during severe plastic deformation*, *Annu. Rev. Mater. Res.* **40**, 319 (2010).
- [18] O. Renk and R. Pippan, *Saturation of grain refinement during severe plastic deformation of single phase materials: Reconsiderations, current status and open questions*, *Mater. Trans.* **60**, 1270 (2019).
- [19] P. C. J. Gallagher, *The influence of alloying, temperature, and related effects on the stacking fault energy*, *Metall. Mater. Trans. B* **1**, 2429 (1970).
- [20] T. Ericsson, *The temperature and concentration dependence of the stacking fault energy in the Co-Ni system*, *Acta Metall.* **14**, 853 (1966).
- [21] C. W. Shao, P. Zhang, R. Liu, Z. J. Zhang, J. C. Pang, Q. Q. Duan, and Z. F. Zhang, *A remarkable improvement of low-cycle fatigue resistance of high-Mn austenitic TWIP alloys with similar tensile properties: Importance of slip mode*, *Acta Mater.* **118**, 196 (2016).
- [22] C. N. J. Wagner, *Stacking faults by low-temperature cold work in copper and alpha brass*, *Acta Metall.* **5**, 427 (1957).
- [23] A. K. Majumdar and P. von Blanckenhagen, *Magnetic phase diagram of $Fe_{80-x}Ni_xCr_{20}$ ($10 \leq x \leq 30$) alloys*, *Phys. Rev. B* **29**, 4079 (1984).
- [24] A. Reyes-Huamantínco, P. Puschnig, C. Ambrosch-Draxl, O. E. Peil, and A. V. Ruban, *Stacking-fault energy and anti-Invar effect in Fe-Mn alloy from first principles*, *Phys. Rev. B* **86**, 060201(R) (2012).
- [25] A. V. Ruban and M. Dehghani, *Atomic configuration and properties of austenitic steels at finite temperature: Effect of longitudinal spin fluctuations*, *Phys. Rev. B* **94**, 104111 (2016).
- [26] O. K. Andersen, O. Jepsen, and G. Krier, *Exact muffin-tin orbital theory*, in *Lectures on Methods of Electronic Structure Calculations*, edited by V. Kumar, O. K. Andersen, and A. Mookerjee (World Scientific Publishing Co., Singapore, 1995), pp. 63–124.
- [27] L. Vitos, *Computational Quantum Mechanics for Materials Engineers* (Springer Verlag, London, 2007).
- [28] P. Soven, *Coherent-potential model of substitutional disordered alloys*, *Phys. Rev.* **156**, 809 (1967).
- [29] B. L. Gyorffy, *Coherent-potential approximation for a nonoverlapping-muffin-tin-potential model of random substitutional alloys*, *Phys. Rev. B* **5**, 2382 (1972).
- [30] L. Vitos, I. A. Abrikosov, and B. Johansson, *Anisotropic Lattice Distortions in Random Alloys from First-Principles Theory*, *Phys. Rev. Lett.* **87**, 156401 (2001).
- [31] I. A. Abrikosov, A. M. N. Niklasson, S. I. Simak, B. Johansson, A. V. Ruban, and H. L. Skriver, *Order- N Green's Function Technique for Local Environment Effects in Alloys*, *Phys. Rev. Lett.* **76**, 4203 (1996).

- [32] I. Abrikosov, S. Simak, B. Johansson, A. Ruban, and H. Skriver, Locally self-consistent Green's function approach to the electronic structure problem, *Phys. Rev. B* **56**, 9319 (1997).
- [33] O. E. Peil, A. V. Ruban, and B. Johansson, Self-consistent supercell approach to alloys with local environment effects, *Phys. Rev. B* **85**, 165140 (2012).
- [34] J. P. Perdew and Y. Wang, Accurate and simple analytic representation of the electron-gas correlation energy, *Phys. Rev. B* **45**, 13244 (1992).
- [35] J. P. Perdew, K. Burke, and M. Ernzerhof, Generalized Gradient Approximation Made Simple, *Phys. Rev. Lett.* **77**, 3865 (1996).
- [36] A. V. Ruban, On segregation in multicomponent alloys: Surface segregation in austenite and FeCr-CoNiMn alloys, *Comput. Mater. Sci.* **187**, 110080 (2021).
- [37] V. I. Razumovskiy, A. Reyes-Huamantínco, P. Puschnig, and A. V. Ruban, Effect of thermal lattice expansion on the stacking fault energies of fcc Fe and Fe₇₅Mn₂₅ alloy, *Phys. Rev. B* **93**, 054111 (2016).
- [38] D. Scheiber, K. Prabit, L. Romaner, and W. Ecker, The influence of alloying on Zn liquid metal embrittlement in steels, *Acta Mater.* **195**, 750 (2020).